LeTera: Stochastic Beam Control Through ESN Learning in Terahertz-Band Wireless UAV Networks

Sabarish Krishna Moorthy and Zhangyu Guan
Department of Electrical Engineering
State University of New York (SUNY) at Buffalo, Buffalo, NY 14260, USA
Email: {sk382, guan}@buffalo.edu

***Abstract*—Terahertz (THz)-band communication is a key technology to achieve ultra-high-data-rate wireless links in beyond-5G wireless networks. A main challenge with this frequency band is that the wireless links can be easily disconnected because of beam misalignment in mobile environments. This paper focuses on beam control in THz-band wireless Unmanned Aerial Vehicle (UAV) networks, where perfect beam alignment is hard to achieve in the presence of multi-scale mobility uncertainties of the flying UAVs. We propose a learning-based stochastic beam control scheme called *LeTera* to reduce the outage probability of the THz-band wireless links based on Echo State Networks (ESN). The scheme dynamically predicts through echo state learning the best beam width based on statistical information of the UAV mobility pattern. The scheme is evaluated using mobility traces collected through a series of UAV flight field experiments in different weather. Results show that *LeTera* can predict the optimal beam width with 99% accuracy and nearly optimal link capacity can be achieved in the presence of beam alignment latency.**

***Index Terms*—THz-band Communications, Beam Control, Wireless UAV Networks, Echo State Learning.**

I. Introduction

This paper investigates the challenges towards achieving high-data-rate wireless UAV networking in the THz-band (from 0.1 THz to 10 THz). THz-band UAV networks have been envisioned as a key technology to enable a wide set of new applications, including distributed beamforming with collaborative drones [1], distributed aerial edge computing [2], high-throughput and secure tactical wireless networking in contested environments [3], wireless backhauling for cellular networks with mobile hotspots [4]–[6], among others. However, radio in-air signal propagation in this frequency band suffers from significantly high path loss ($0.6 - 1000$ dB/km) due to the absorption by water vapor and oxygen. To overcome this problem, directional transmissions with narrow beams have been used to achieve extended communication distance [7]. The resulting THz-band wireless links can be easily disconnected by the misalignment between the communicating nodes particularly when they are both mobile as in wireless UAV networks.

To address this challenge, beam alignment in high frequency range has attracted significant research efforts in existing literature [8]–[18]. For example, in [8] Ke et. al propose a fast beam tracking scheme based on an efficient position prediction of multiple moving UAVs. Similarly, BeamSpy [9] and Agile-Link [10] predict the best mmWave beam alignment without scanning the space thereby reducing the overhead and delay. In [11], the authors Hashemi et. al design an optimal algorithm to reduce the overhead of beam alignment in mmWave systems. Kovalchukov et. al [18] analyze the effects of directionality and random heights on UAV-based mmWave communications. In [17], Petrov et. al investigate the behavior of THz band wireless links in the presence of small scale mobility of the user. Please refer to [13]–[16] and references therein for an excellent survey of the main results in this field.

The above discussed beam alignment schemes aim at identifying the transmit and receive beams that can result in the highest signal strength, and have not explicitly considered the mobility uncertainties of the flying UAVs. In UAV networks, in addition to the large-scale maneuver, the UAVs also experience small-scale mobility because of the random wind effects and micro-scale mobility caused by the UAV engine operation and propeller rotation. The beam search latency with commercial 60 GHz mmWave routers [19] is at the level of tens of milliseconds, which is comparable with the time scale of the small scale mobility according to the field measurements in our prior research [20]. The situation will get even worse when it goes to the THz band with order of magnitude larger beam search space. As a result, the THz-band wireless links between flying UAVs can be frequently disconnected in the presence of large beam alignment latency.

Contributions. In this paper, we design new beam control approaches for wireless UAV communications in the THz frequency band to reduce the link outage probability in the presence of beam alignment latency. We claim the following three main contributions.

- We propose a stochastic beam control scheme called *LeTera*, which predicts through echo state learning the optimal beam width by jointly considering the distance between the transmit and receive UAVs and the statistical information of their mobility uncertainties.
- We conduct a new set of field experiments to measure the micro-, small- and large-scale mobility uncertainties of flying UAVs. Different weather (normal day and windy day) has been considered in the measurements.
- Based on the measured UAV flight traces, we evaluate the performance of the proposed beam control scheme through an extensive simulation campaign. Results show that *LeTera* can predict the optimal beam width with 99% accuracy and the outage probability of the THz-band link can be significantly reduced in mobile environments.

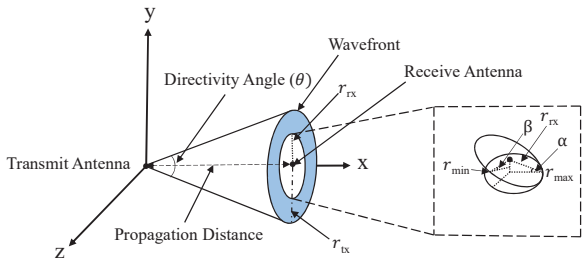

Fig. 1: Cone antenna model for THz signal propagation in the presence of misalignment between transmit and receive antennas.

All the data and code generated through the experiments have been released via GitHub [21].

II. System Model

Consider THz-band wireless communications between two flying UAVs, Tx and Rx. The transmission time is divided into a set $\mathcal{T}$ of time slots. Define $\mathbf{cod}_{\rm tx}^t = (x_{\rm tx}^t,\ y_{\rm tx}^t,\ z_{\rm tx}^t)$ as the coordinate vector of UAV Tx in time slot $t \in \mathcal{T}$, with $x_{\rm tx}^t$, $y_{\rm tx}^t$ and $z_{\rm tx}^t$ being the x-, y- and z-axis components, respectively. Similarly, define $\mathbf{cod}_{\rm rx}^t = (x_{\rm rx}^t,\ y_{\rm rx}^t,\ z_{\rm rx}^t)$ as the coordinate vector of UAV Rx. Let $\eta_{\rm tz}$ denote the signal-to-noise ratio (SNR) of the THz-band link, then the link capacity $C_{\rm tz}$ can be written as

$$C_{\rm tz} = B_{\rm tz}\log_2(1+\eta_{\rm tz}), \tag{1}$$

where $B_{\rm tz}$ is the bandwidth of the transmitted signal. To derive the mathematical expression of $\eta_{\rm tz}$ in (1), we first describe the antenna and channel models.

Antenna Model. We consider as in [22] a cone antenna model for the UAVs. Denote θ as the directivity angle of the transmit antenna, then the radius of the transmit wavefront, denoted as $r_{\rm tx}$, can be written as

$$r_{\rm tx} = \tan\left(\frac{\theta}{2}\times\frac{\pi}{180}\right) d(\mathbf{cod}_{\rm rx}^t,\ \mathbf{cod}_{\rm tx}^t), \tag{2}$$

where $d(\mathbf{cod}_{\rm rx}^t, \mathbf{cod}_{\rm tx}^t)$ is the propagation distance defined as

$$\begin{aligned} &d(\mathbf{cod}_{\rm rx}^t,\ \mathbf{cod}_{\rm tx}^t) \\ &\quad=\sqrt{(x_{\rm rx}^t - x_{\rm tx}^t)^2 + (y_{\rm rx}^t - y_{\rm tx}^t)^2 + (z_{\rm rx}^t - z_{\rm tx}^t)^2}. \end{aligned} \tag{3}$$

The area of the transmit wavefront, denoted as $A_{\rm tx}$, can then be given as

$$A_{\rm tx} = \pi r_{\rm tx}^2, \tag{4}$$

with $r_{\rm tx}$ being the radius of the transmit wavefront in (2).

Without loss of generality, as illustrated in Fig. 1, consider UAV Tx's location as the origin, i.e., $\mathbf{cod}_{\rm tx}^t = (0,\ 0,\ 0)$. Then the propagation distance $d(\mathbf{cod}_{\rm rx}^t,\ \mathbf{cod}_{\rm tx}^t)$ in (3) can be redefined as $d(\mathbf{cod}_{\rm rx}^t) \triangleq d(\mathbf{cod}_{\rm rx}^t,\ (0,\ 0,\ 0))$. The effective receiving area of UAV Rx's antenna depends on the time-varying relative locations as well as the rotation and inclination angles of the two UAVs. Let α and β denote the relative roll and pitch angles of UAV Rx's antenna with respect to y- and z-axis, respectively. Then the receiving area $A_{\rm rx}$ can be written as

$$A_{\rm rx} = \pi r_{\min} r_{\max} \tag{5}$$

where $r_{\min} = r_{\rm rx}\cos\beta$ and $r_{\max} = r_{\rm rx}\cos\alpha$ are the minor and major axes of the elliptical projection of receive antenna surface onto the y-z plane. Since in each time slot $t \in \mathcal{T}$ UAV Rx's antenna may or may not overlap completely UAV Tx's wavefront, let $A_{\rm rx}^{\rm ovlp} = A_{\rm tx} \cap A_{\rm rx}$ represent the effective receiving area of UAV Rx's antenna, with $A_{\rm tx}$ and $A_{\rm rx}$ defined in (4) and (5), respectively.

Channel Model. Let $f_{\rm tz}$ and $B_{\rm tz}$ denote the central frequency and bandwidth of the signal, respectively. For $f \in [f_{\rm tz} - \frac{B_{\rm tz}}{2} \quad f_{\rm tz} + \frac{B_{\rm tz}}{2}]$, let $S_{\rm tx}(f)$ represent the single-sided power spectral density (p.s.d). Then the power of the transmitted signal at the receive antenna, denoted as $P_{\rm tx}$, can be given as

$$P_{\rm tx} = \lambda(\mathbf{cod}_{\rm rx}^t)\int_{f_{\rm tz}-\frac{B_{\rm tz}}{2}}^{f_{\rm tz}+\frac{B_{\rm tz}}{2}} S_{\rm tx}(f)df, \tag{6}$$

where $\lambda(\mathbf{cod}_{\rm rx}^t) = \frac{1}{A_{\rm tx}}$ is the spreading attenuation coefficient with propagation distance $d(\mathbf{cod}_{\rm rx}^t)$, with $A_{\rm tx}$ being the transmit wavefront area defined in (4).

The THz-band frequency response of the wireless channel, denoted as $H_{\rm tz}(f, d(\mathbf{cod}_{\rm rx}^t))$ at frequency f and propagation distance $d(\mathbf{cod}_{\rm rx}^t)$, can be given as

$$H_{\rm tz}(f, d(\mathbf{cod}_{\rm rx}^t)) = \left|\frac{c}{4\pi d(\mathbf{cod}_{\rm rx}^t)}\int_{f_{\rm tz}-\frac{B_{\rm tz}}{2}}^{f_{\rm tz}+\frac{B_{\rm tz}}{2}} \frac{e^{-\frac{\mu(f)d(\mathbf{cod}_{\rm rx}^t)}{2}}}{f}\right|^2 df, \tag{7}$$

where c is the speed of light and $\mu(f)$ is the molecular absorption coefficient for THz signal of frequency f. Then the received power at UAV Rx, denoted as $P_{\rm rx}$, can be expressed as [23]

$$P_{\rm rx} = A_{\rm rx}^{\rm ovlp} P_{\rm tx} H_{\rm tz}(f, d(\mathbf{cod}_{\rm rx}^t))|H_{\rm rx}(f)|^2, \tag{8}$$

where $P_{\rm tx}$ and $H_{\rm tz}(f, d(\mathbf{cod}_{\rm rx}^t))$ are defined in (6) and (7), respectively; $H_{\rm rx}(f)$ denotes the frequency response of the receive antenna and is considered to be an ideal low-pass filter with bandwidth $B_{\rm tz}$.

Finally, the molecular absorption noise is correlated to the transmitted signal, i.e., there is only background noise unless the molecules are irradiated. Moreover, different molecules resonate at different frequencies and their resonance is not confined to a single frequency but spreads over a narrow band. As a result, the power spectral density (p.s.d.) of the noise has several peaks in frequency. The total receiver noise at propagating distance $d(\mathbf{cod}_{\rm rx}^t)$, denoted as $N_{\rm rx}$, can then be given as [24]

$$N_{\rm rx} = \int_{f_{\rm tz}-\frac{B_{\rm tz}}{2}}^{f_{\rm tz}+\frac{B_{\rm tz}}{2}} (S_{\rm back}(f) + S_{\rm self})|H_{\rm rx}|^2 df, \tag{9}$$

where $S_{\rm back}(f)$ is the background atmospheric noise p.s.d, $S_{\rm self}$ is self-induced noise p.s.d, and $H_{\rm rx}$ is the receive antenna

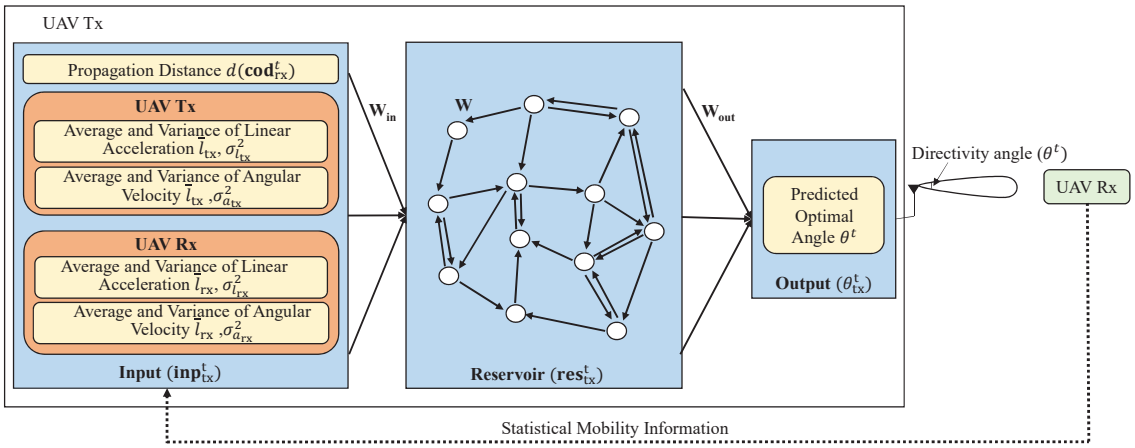

Fig. 2: *LeTera*: A Learning-based Stochastic Beam Control Scheme.

frequency response. Then, the SNR of the THz link, i.e., $\eta_{\rm tz}$ in (1), can be given as $\eta_{\rm tz} = \frac{P_{\rm rx}}{N_{\rm rx}}$, with $P_{\rm rx}$ and $N_{\rm rx}$ defined in (8) and (9), respectively.

III. Beam Control Algorithm

The objective of beam control is to maximize the THz link capacity $C_{\rm tz}$ in (1) by determining the optimal directivity angle θ in each time slot $t \in \mathcal{T}$. As discussed in Section II, the directivity angle θ is one of the key factors that affect the link capacity. On one hand, larger angle results in larger transmit wavefront area $A_{\rm tx}$ and hence lower power density $S_{\rm tx}(f)$ and lower received SNR $\eta_{\rm tz}$. On the other hand, smaller angle leads to smaller effective receiving area $A^{\rm ovlp}_{\rm rx}$ and hence will cause more frequent misalignment between the transmit and receive antennas.

The main challenge is to determine the optimal directivity angle in each time slot in the presence of small- and large-scale mobility uncertainties of both the Tx and Rx UAVs [20]. To address this challenge, in this paper we propose a learning-based stochastic beam control scheme called *LeTera*, which determines the optimal angle through echo state learning based on the statistical UAV mobility information. Compared to traditional neural networks, which are computationally expensive, it is incredibly simple to train ESNs, while they are still able to model the complex time-varying behaviors of dynamical systems. The diagram of *LeTera* is illustrated in Fig. 2, which consists of three modules: *Input*, *Reservoir* and *Output*.

Input Design. The input of the *LeTera* ESN comprises of the mobility information of UAV Tx and UAV Rx. This information includes the propagation distance, the average and variance of the location displacement of UAVs Tx and Rx, the average and variance of their roll, pitch and yaw angles. Since the statistical information of the UAVs' mobility changes only slowly with time and hence no frequent feedback is needed, the communication overhead of *LeTera* can be significantly reduced.

The location displacement of UAV Tx and UAV Rx at time slot $t+1$ with respect to time slot t can be expressed respectively as

$$l^{t+1}_{\rm tx} = \sqrt{(x^{t+1}_{\rm tx} - x^t_{\rm tx})^2 + (y^{t+1}_{\rm tx} - y^t_{\rm tx})^2 + (z^{t+1}_{\rm tx} - z^t_{\rm tx})^2}, \quad (10)$$

$$l^{t+1}_{\rm rx} = \sqrt{(x^{t+1}_{\rm rx} - x^t_{\rm rx})^2 + (y^{t+1}_{\rm rx} - y^t_{\rm rx})^2 + (z^{t+1}_{\rm rx} - z^t_{\rm rx})^2}. \quad (11)$$

Then, the average location displacement, denoted respectively as $\bar{l}_{\rm tx}$ and $\bar{l}_{\rm rx}$ for UAVs Tx and Rx, can be given as

$$\bar{l}_{\rm tx} = \frac{1}{\mathcal{T}} \sum_{t \in \mathcal{T}} l^{t+1}_{\rm tx}, \quad (12)$$

$$\bar{l}_{\rm rx} = \frac{1}{\mathcal{T}} \sum_{t \in \mathcal{T}} l^{t+1}_{\rm rx}. \quad (13)$$

The corresponding variance of the location displacement, denoted as $\sigma^2_{l_{\rm tx}}$ and $\sigma^2_{l_{\rm rx}}$, can be written as

$$\sigma^2_{l_{\rm tx}} = \frac{1}{\mathcal{T}} \sum_{t \in \mathcal{T}} (l^{t+1}_{\rm tx} - \bar{l}_{\rm tx})^2, \quad (14)$$

$$\sigma^2_{l_{\rm rx}} = \frac{1}{\mathcal{T}} \sum_{t \in \mathcal{T}} (l^{t+1}_{\rm rx} - \bar{l}_{\rm rx})^2. \quad (15)$$

Similarly, let $(\alpha^t_{\rm tx}, \beta^t_{\rm tx}, \gamma^t_{\rm tx})$ and $(\alpha^t_{\rm rx}, \beta^t_{\rm rx}, \gamma^t_{\rm rx})$ denote the roll, pitch and yaw angles of UAV Rx at time slot t, and $(\alpha^{t+1}_{\rm tx}, \beta^{t+1}_{\rm tx}, \gamma^{t+1}_{\rm tx})$ and $(\alpha^{t+1}_{\rm rx}, \beta^{t+1}_{\rm rx}, \gamma^{t+1}_{\rm rx})$ denote the angles at time slot $t+1$. Then the average (denoted respectively as $\bar{a}_{\rm tx}$ and $\bar{a}_{\rm rx}$ for UAVs Tx and Rx) and variance (denoted as $\sigma^2_{a_{\rm tx}}$ and $\sigma^2_{a_{\rm rx}}$) of the angular displacement can be calculated similar to (12)-(15). It is worth pointing out that we consider the average and variance of the overall angular displacement instead of the individual angular components as the input to the ESN, because we want to keep the input dimension of the ESN to a minimum while without degrading the prediction accuracy of the ESN.

Finally, the input to the *LeTera* ESN at time t, represented as $\mathbf{inp}^t_{\rm tx}$, can be defined as

$$\mathbf{inp}^t_{\rm tx} = (d(\mathbf{cod}^t_{\rm rx}), \bar{l}_{\rm tx}, \bar{l}_{\rm rx}, \sigma^2_{l_{\rm tx}}, \sigma^2_{l_{\rm rx}}, \bar{a}_{\rm tx}, \bar{a}_{\rm rx}, \sigma^2_{a_{\rm tx}}, \sigma^2_{a_{\rm rx}}, \theta^t_{\rm tgt}), \quad (16)$$

where $\theta^t_{\rm tgt}$ is the target directivity angle in time slot t and is needed only for training the *LeTera* ESN. In this work, $\theta^t_{\rm tgt}$ is obtained based on grid search in the training phase.

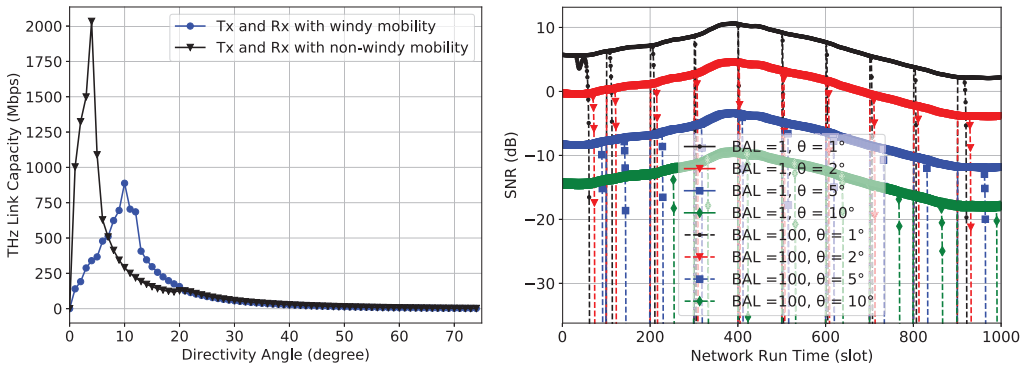

(a) (b)

Fig. 3: (a) Link capacity with different beam directivity angles; (b) Link SNR with different beam alignment latency (BAL).

Reservoir Design. In echo state learning a reservoir acts as a nonlinear high-dimensional expansion and a memory of input $\mathbf{inp}_{\text{tx}}^t$ [25]. The reservoir provides a rich and relevant enough signal space $\mathbf{res}_{\text{tx}}^t \in \mathbb{R}^{N_{\text{res}}}$ with N_{res} being the dimension of the reservoir units (the small circles in Reservoir $\mathbf{res}_{\text{tx}}^t$ in Fig. 2), in which the desired output θ_{tgt}^t can be represented by linear combination of $\mathbf{inp}_{\text{tx}}^t$ and $\mathbf{res}_{\text{tx}}^t$. Let N_{inp} and N_{out} denote the dimension of the input and output units, respectively. Given the training input signal $\mathbf{inp}^t \in \mathbb{R}^{N_{\text{inp}}}$ and the target output signal $\theta_{\text{tgt}}^t \in \mathbb{R}^{N_{\text{out}}}$, the objective of *LeTera* in the training phase is to learn a model with output θ^t that minimizes the root-mean-square error (RMSE) between θ^t and θ_{tgt}^t, defined as

$$E(\theta^t, \theta_{\text{tgt}}^t) = \frac{1}{N_{\text{out}}} \sum_{i=1}^{N_{\text{out}}} \sqrt{\frac{1}{|\mathcal{T}|} \sum_{t=1}^{|\mathcal{T}|} (\boldsymbol{\theta}^t - \theta_{\text{tgt}}^t)^2}, \tag{17}$$

where $|\cdot|$ represents the cardinality of a set.

For the signal space $\mathbf{res}_{\text{tx}}^t$, *LeTera* uses a Recurrent Neural Network (RNN) with leaky-integrated discrete-time continuous-value units. Let $\mathbf{W_{in}} \in \mathbb{R}^{N_{\text{res}} \times (1+N_{\text{inp}})}$ and $\mathbf{W} \in \mathbb{R}^{N_{\text{res}} \times N_{\text{res}}}$ denote the input and reservoir weight matrices, respectively. Further let $\delta \in (0, 1]$ denote the leaking rate. Then, in *LeTera* the signal space $\mathbf{res}_{\text{tx}}^t$ can be updated as

$$\widetilde{\mathbf{res}}_{\text{tx}}^t = \tanh(\mathbf{W_{in}}[1; \mathbf{inp}_{\text{tx}}^t] + \mathbf{W}\mathbf{res}_{\text{tx}}^{t-1}), \tag{18}$$

$$\mathbf{res}_{\text{tx}}^t = (1 - \delta)\, \mathbf{res}_{\text{tx}}^{t-1} + \delta\, \widetilde{\mathbf{res}}_{\text{tx}}^t \tag{19}$$

where $\tanh(\cdot)$ is the transfer function, and $[\cdot;\cdot]$ stands for matrix concatenation operation. Then the output θ^t can be given as

$$\theta^t = \mathbf{W_{out}}[1; \mathbf{inp}_{\text{tx}}^t; \mathbf{res}_{\text{tx}}^t], \tag{20}$$

where $\mathbf{W_{out}} \in \mathbb{R}^{N_{out} \times (1+N_{\text{inp}}+N_{\text{res}})}$ is the output weight matrix of the *LeTera* ESN.

Output Design. The output of *LeTera* is the predicted optimal directivity angle θ for UAV Tx in each time slot $t \in \mathcal{T}$, denoted as θ^t.

IV. Performance Evaluation

We evaluate the performance of *LeTera* based on mobility traces collected through a series of field experiments. In the experiments an Intel Aero Ready-to-Fly (RtF) drone is used to carry an Android smartphone with inbuilt linear acceleration and gyroscope sensors. Two sets of experiments are conducted in outdoor environments with different weather: *normal day* and *windy day*. Sensor Kinetics Pro App is used to record the measured mobility data, including the angular velocity of the orientation and rotation of UAV, and the acceleration of the UAV movement excluding the effect of gravity of Earth. A set of 10 traces have been recorded, with each trace lasting 10 seconds. Based on the measured UAV mobility traces, we evaluate the performance of *LeTera* in terms of prediction accuracy and link capacity. The center frequency of the THz link is set to f_{tz} = 300 GHz and the bandwidth is set to B_{tz} = 10 GHz. Each run of the simulation lasts $\mathcal{T}$ = 1000 time slots, with time slot duration of 5 ms. The data set and source code have been released via GitHub [21].

Effects of Beam Control. In this experiment we first study the effects of directivity angle on the THz-band link capacity. Two mobility traces are considered in windy and non-windy weather, respectively. The directivity angle is varied from 1 to 75 degrees with step of 1 degree. For each angle, the link capacity is averaged over all the time slots for each mobility trace. The results are reported in Fig. 3(a). It can be seen that when UAVs are flying in non-windy environments, the maximum THz link capacity (around 2 Gbps) is achieved with directivity angle of 4°. Differently, when they are flying in windy weather the maximum capacity (around 1 Gbps) is achieved with directivity angle of 10°. This is because in windy environments the UAVs experience more frequent small-scale fluctuations, and larger directivity angles can lead to lower link outage probability. This verifies the importance of dynamically adapting the directivity angle to the UAV's mobility uncertainties.

We further investigate the effects of directivity angles on the SNR of the THz-band link with different beam alignment latency (BAL). The mobility trace in windy weather is considered as an example. We consider BAL of 1 and 100 time slots (corresponding to 5 ms and 500 ms, respectively) and calculate the SNR of the THz link with directivity angles of 1, 2, 5 and 10 degrees. The results are given in Fig. 3(b). With BAL of 1 time slot, the highest SNR (on average 6.5 dB)

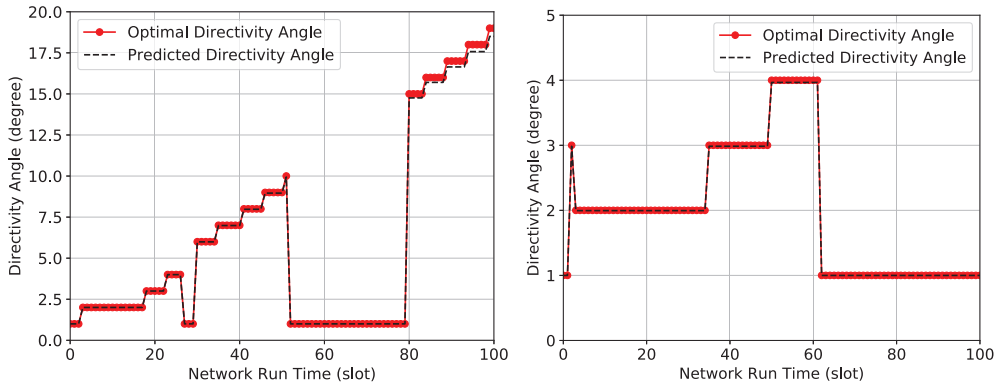

Fig. 4: Prediction accuracy of *LeTera* in (a) windy and (b) non-windy environments.

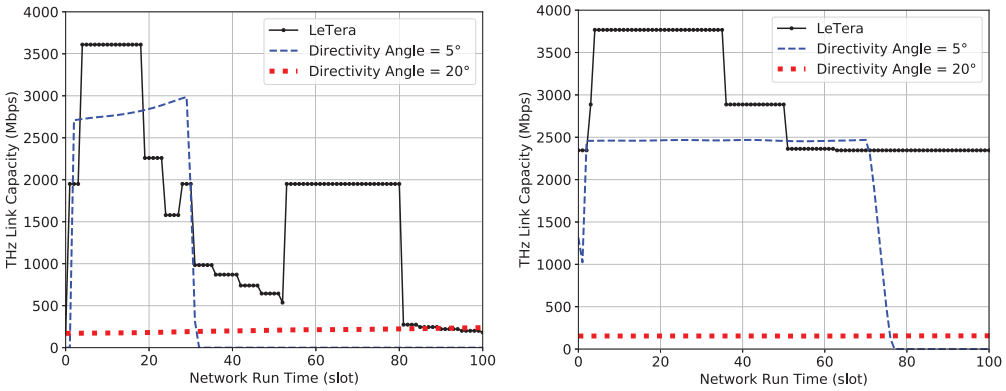

Fig. 5: Link capacity with different directivity angles in (a) windy and (b) non-windy environments.

is achieved with directivity angle of $1°$. This is because the THz link can recover from the misalignment almost in real time, and hence higher SNR can be achieved by transmitting with smaller directivity angle to concentrate better the signal energy. However, with BAL of 100 time slots (i.e., 500 ms), we can see that the THz-band link is disconnected frequently (with probability of 39%-87%), because of the misalignment caused by the large- and small-scale mobility of the UAVs in windy weather.

Prediction Accuracy. In the following experiments we will test the effectiveness of the proposed *LeTera* scheme in terms of prediction accuracy and the achievable link capacity. In order to show the accuracy of the designed *LeTera* algorithm, we train and test the ESN model with input data (as defined in (16)) collected in 1000 time slots. The first 90% of the input data is used for training and the remaining is used for testing. As discussed in Section III, we first determine the optimal directivity angle with the highest link capacity, through exhaustive grid search over different directivity angles. The resulting optimal angles are used as the target output θ^t_{tgt} for minimizing the RMSE in (17). The prediction accuracy of the ESN is defined as $1 - |\theta^t - \theta^t_{\text{tgt}}|/\theta^t_{\text{tgt}}$, where θ^t is the predicted beam angle. The results are shown in Figs. 4(a) and (b) for UAVs flying in non-windy and windy weather, respectively. We can see that *LeTera* is able to predict the optimal directivity angle with very high accuracy. For example, in Fig. 4(a) an accuracy of 99% can be achieved in windy environments.

Link Capacity Results. In Fig. 5 we plot the link capacity achieved by *LeTera* and two benchmark schemes with fixed directivity angles of $5°$ and $20°$. Beam alignment latency is set to 100 time slots for all the three schemes. We can see that a significant gain in terms of average link capacity can be achieved by *LeTera*. For example, in windy weather (Fig. 5(a)) an average link capacity of 1.574 Gbps can be achieved by *LeTera*, compared to 0.794 Gbps and 0.204 Gbps for the benchmark schemes. Particularly, from 50 to 80 time slots the link is completely disconnected with directivity angle of $5°$, while *LeTera* can still achieve a link capacity close to 2 Gbps.

In Fig. 6 we plot the THz link capacity achieved by *LeTera* with beam alignment latency of 1, 5, 10, 25 and 50 time slots. The case with latency of 1 time slot is considered as the optimal beam alignment scheme. From Fig. 6(a), where the UAVs fly in the windy environments, it can be seen that nearly optimal (over 99%) link capacity can be achieved with beam alignment latency of 5 and 10 time slots (25 ms and 50 ms, respectively). Similarly, in non-windy weather (Fig. 6(b)), over 99% and 97% of the optimal link capacity can be achieved when the beam alignment latency is 10 and 25 time slots, respectively. This verifies the effectiveness of *LeTera* in improving the robustness of the THz-band wireless links in the presence of beam alignment latency.

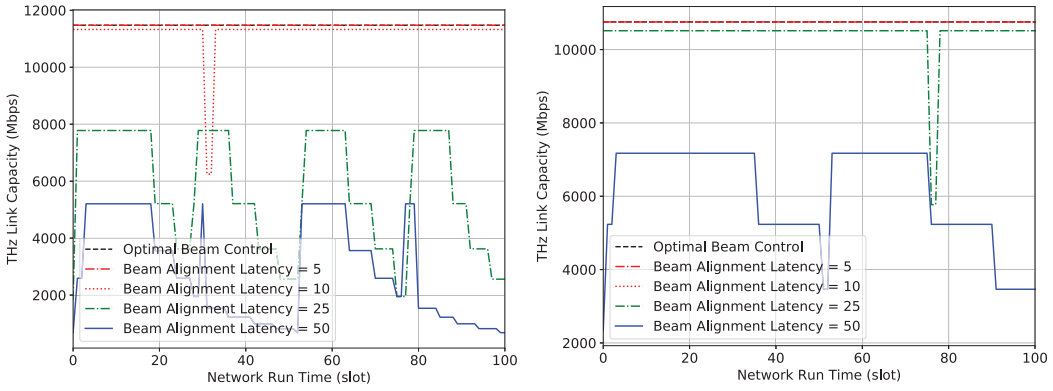

Fig. 6: Link capacity with different beam alignment latency in (a) windy and (b) non-windy environments.

V. CONCLUSION

In this paper, we have studied the problem of adaptive beam control for wireless UAV communications in the THz bands. We proposed a stochastic beam control scheme called *LeTera*, which can predict through echo state learning the optimal beam directivity angle based on second-order moment of the mobility pattern of the UAVs. We evaluated the effectiveness of *LeTera* through an extensive simulation campaign. Results indicate that *LeTera* can predict the optimal beam directivity angle with very high accuracy (over 99%), and can achieve nearly optimal link capacity with beam alignment latency of up to 50 ms. The dataset of UAV flight traces and source code have released to the community via GitHub for repeating the experiments.

REFERENCES

[1] Z. Guan, N. Cen, T. Melodia, and S. Pudlewski, "Self-Organizing Flying Drones with Massive MIMO Networking," in *Proc. of Mediterranean Ad Hoc Networking Workshop (Med-Hoc-Net)*, Capri, Italy, June 2018.

[2] N. Cheng, W. Xu, W. Shi, Y. Zhou, N. Lu, H. Zhou, and X. Shen, "Air-Ground Integrated Mobile Edge Networks: Architecture, Challenges and Opportunities," *IEEE Commun. Magazine*, vol. 56, no. 8, pp. 26–32, August 2018.

[3] L. Zhang, Z. Guan, and T. Melodia, "United Against the Enemy: Anti-Jamming Based on Cross-Layer Cooperation in Wireless Networks," *IEEE Transactions on Wireless Communications*, vol. 15, no. 8, pp. 5733–5747, Aug 2016.

[4] I. Bor-Yaliniz and H. Yanikomeroglu, "The New Frontier in RAN Heterogeneity: Multi-Tier Drone-Cells," *IEEE Commun. Magazine*, vol. 54, no. 11, pp. 48–55, Nov. 2016.

[5] H. Wang, G. Ding, F. Gao, J. Chen, J. Wang, and L. Wang, "Power Control in UAV-Supported Ultra Dense Networks: Communications, Caching, and Energy Transfer," *IEEE Commun. Magazine*, vol. 56, no. 6, pp. 28–34, June 2018.

[6] Y. Zeng, R. Zhang, and T. J. Lim, "Wireless Communications with Unmanned Aerial Vehicles: Opportunities and Challenges," *IEEE Commun. Magazine*, vol. 54, no. 5, pp. 36–42, May 2016.

[7] K. Heimann, J. Tiemann, S. Boecker, and C. Wietfeld, "On the Potential of 5G mmWave Pencil Beam Antennas for UAV Communications: An Experimental Evaluation," in *Proc. of International ITG Workshop on Smart Antennas (WSA)*, Bochum, Germany, March 2018.

[8] Y. Ke, H. Gao, W. Xu, L. Li, L. Guo, and Z. Feng, "Position Prediction Based Fast Beam Tracking Scheme for Multi-User UAV-mmWave Communications," in *Proc. of IEEE ICC*, Shanghai, China, May 2019.

[9] S. Sur, X. Zhang, P. Ramanathan, and R. Chandra, "BeamSpy: Enabling Robust 60 GHz Links Under Blockage," in *Proc. of Symposium on Networked Systems Design and Implementation (NSDI 16)*, Santa Clara, CA, March 2016.

[10] H. Hassanieh, O. Abari, M. Rodriguez, M. Abdelghany, D. Katabi, and P. Indyk, "Fast Millimeter Wave Beam Alignment," in *Proc. of Conference of the ACM Special Interest Group on Data Commun.*, Budapest, Hungary, August 2018.

[11] M. Hashemi, A. Sabharwal, C. E. Koksal, and N. B. Shroff, "Efficient Beam Alignment in Millimeter Wave Systems Using Contextual Bandits," in *Proc. of IEEE ICC*, Honolulu, HI, April 2018.

[12] M. K. Haider, Y. Ghasempour, D. Koutsonikolas, and E. W. Knightly, "LiSteer: MmWave Beam Acquisition and Steering by Tracking Indicator LEDs on Wireless APs," in *Proc. of International Conference on Mobile Computing and Networking*, New Delhi, India, Oct. 2018.

[13] S. Kutty and D. Sen, "Beamforming for Millimeter Wave Communications: An Inclusive Survey," *IEEE Commun. Surveys Tutorials*, vol. 18, no. 2, pp. 949–973, December 2016.

[14] Z. Xiao, P. Xia, and X.-G. Xia, "Enabling UAV Cellular with Millimeter-Wave Communication: Potentials and Approaches," *IEEE Commun. Magazine*, vol. 54, no. 5, pp. 66–73, May 2016.

[15] S. Mumtaz, J. Jornet, J. Aulin, W. Gerstacker, X. Dong, and b. ai, "Terahertz Communication for Vehicular Networks," *IEEE Trans. on Vehicular Technology*, vol. 66, no. 7, pp. 5617–5624, July 2017.

[16] M. Xiao, S. Mumtaz, Y. Huang, L. Dai, Y. Li, M. Matthaiou, G. K. Karagiannidis, E. Björnson, K. Yang, C. I, and A. Ghosh, "Millimeter Wave Communications for Future Mobile Networks," *IEEE Journal on Selected Areas in Commun.*, vol. 35, no. 9, pp. 1909 – 1911, Sept. 2017.

[17] V. Petrov, D. Moltchanov, Y. Koucheryavy, and J. M. Jornet, "The Effect of Small-Scale Mobility on Terahertz Band Communications," in *Proc. ACM/IEEE International Conference on Nanoscale Computing and Commun. (NanoCom)*, Reykjavik, Iceland, Sept. 2018.

[18] R. Kovalchukov, D. Moltchanov, A. Samuylov, A. Ometov, S. Andreev, Y. Koucheryavy, and K. Samouylov, "Analyzing Effects of Directionality and Random Heights in Drone-based mmWave Communication," *IEEE Transactions on Vehicular Technology*, vol. 67, no. 10, pp. 10 064–10 069, Oct. 2018.

[19] "TP-Link. 2018. talon ad7200 multi-band router." [Online]. Available: http://www.tp-link. com/en/products/details/AD7200.html. (2018)

[20] Z. Guan and T. Kulkarni, "On the Effects of Mobility Uncertainties on Wireless Communications Between Flying Drones in the mmWave/THz Bands," in *Proc. of IEEE INFOCOM Workshop on Wireless Communications and Networking in Extreme Environments (WCNEE)*, Paris, France, April 2019.

[21] https://github.com/ubwingslab/new-spectrum-technology.

[22] V. Petrov, M. Komarov, D. Moltchanov, J. M. Jornet, and Y. Koucheryavy, "Interference Analysis of EHF/THF Communications Systems with Blocking and Directional Antennas," in *Proc. of IEEE GLOBECOM*, Singapore, Dec. 2016.

[23] J. M. Jornet and I. F. Akyildiz, "Channel Modeling and Capacity Analysis of Electromagnetic Wireless Nanonetworks in The Terahertz Band," *IEEE Transactions on Wireless Commun.*, vol. 10, no. 10, pp. 3211–3221, Oct. 2011.

[24] ——, "Femtosecond-long Pulse-based Modulation for Terahertz Band Communication in Nanonetworks," *IEEE Trans. on Commun.*, vol. 62, no. 5, pp. 1742–1754, May 2014.

[25] M. Lukoševičius, "A Practical Guide to Applying Echo State Networks," *Lecture Notes*, Jan. 2012.